ARTICLE

Molecular Dynamics Simulation of Typical Molecular Ferroelectrics based on Polarized Crystal Charge Model

Ruining Wang[a,b], Feng Xu[a,b], Xiongfei Gui[a,b], Yongle Li[a,b,c*]

a. Department of Physics, Shanghai University, Shanghai 200444, China
b. International Centre for Quantum and Molecular Structures, Shanghai University, Shanghai 200444, China
c. Shanghai Frontiers Science Center of Quantum and Superconducting Matter States, Shanghai University, Shanghai 200444, China

(Dated: Received on April 17, 2022; Accepted on May 12, 2022)

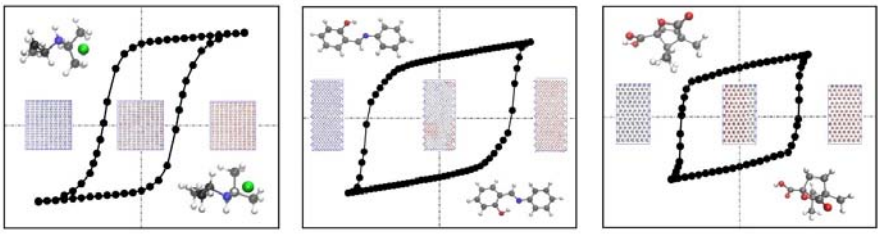

Molecular ferroelectrics are a promising class of ferroelectrics, with environmental friendliness, flexibility and low cost. In this work, a set of characteristic molecular ferroelectrics are simulated by molecular dynamics (MD) with polarized crystal charge (PCC). From the simulated results, their ferroelectric switching mechanisms are elucidated, with their ferroelectric hysteresis loops. The PCC charge model, recently developed by our group, containing the quantum electric polarization effect, is suitable in nature for studying molecular ferroelectrics. The simulated systems include the typical molecular ionic ferroelectrics, di-isopropyl-ammonium halide (DIPAX, X=C (Cl), B (Br), and I), as well as a pair of newly validated organic molecular ferroelectrics, salicylideneaniline and (-)-camphanic acid. In total, there are five systems under investigation. Results demonstrate that the PCC MD method is efficient and reliable. It not only elucidates the ferroelectric switching mechanism of the studied molecular ferroelectrics, but also extends the application range of the PCC MD. In conclusion, PCC MD provides an efficient protocol for extensive computer simulations of molecular ferroelectrics, with reliable ferroelectric properties and associated mechanisms, and would promote further exploration of novel molecular ferroelectrics.

Key words: Molecular ferroelectrics, Molecular dynamics simulation, Modern theory of polarization

I. INTRODUCTION

Ferroelectrics are electroactive materials with spontaneous polarization that can be controlled by electric field, temperature change and mechanical stress [1–3]. They have been widely used in industrial and commercial fields, such as piezoelectric sensing, data storage device, radio and communication filters [4–6]. Among them, molecular ferroelectric crystals are attracting extensive attention from both fundamental research and industry due to their mechanical flexibility, ease of preparation and portability [7, 8]. Especially in recent years, some molecular ferroelectrics are found to be with performance nearly the same as inorganic counterparts traditionally applied such as perovskite [9]. Therefore, they can be used as potential substitutes or comple-

*Author to whom correspondence should be addressed. E-mail: yongleli@shu.edu.cn

ments to traditional inorganic ferroelectrics.

However, the current computational studies on the properties of molecular ferroelectrics are still challenging. Most of the calculations are based on electronic structure calculated from first-principles, but due to the large number of atoms and the complex structure of molecular crystals, the first-principles calculation is hindered by the huge computational complexity. Molecular dynamics (MD) simulation is a powerful tool which can simulate large systems containing millions of atoms [10], but its accuracy is greatly affected by force field parameters. In classical force fields like AMBER [11] and CHARMM [12], the electrostatic interaction within the system is mainly described by Coulomb interaction between fixed partial charges of atoms, which is deficient to simulate molecular crystals due to the missing of electric polarization [13, 14]. Therefore direct usage of force field MD for simulating molecular ferroelectrics would be erroneous.

In order to simulate large scale behaviors, such as polarization switching and associated saturated polarization and coercive electric field of molecular ferroelectrics using MD simulations, our group recently developed the polarized crystal charge (PCC) model [15–17] to simulate the molecular ferroelectrics with both efficiency and accuracy by containing the quantum electric polarization effects, which is indispensable in simulations of molecular crystals. Our method has already been successfully applied into several materials. For example, in our previous work, saturated polarization strength of γ-glycine was 53 $\mu C/cm^2$, which had a relative error of 25% compared with the first-principles calculation result of 70.9 $\mu C/cm^2$ [15]. Besides, the calculated saturated polarization strength of $(R)/(S)$-3-quinuclidinol were 7.4±0.1 and 7.8±0.1 $\mu C/cm^2$, respectively, and the corresponding results from experiments were 6.69 and 6.72 $\mu C/cm^2$. The relative errors were 15% and 10% [16]. These examples validated that PCC MD can give reliable spontaneous polarization values, coercive electric fields, ferroelectric switching mechanism, and Curie temperatures.

To expand the range of applications of PCC, and have an extensive benchmark, in this work, we perform PCC MD to calculate the ferroelectric hysteresis loop and associated switching mechanisms of a set of characteristically ferroelectric materials. Firstly, as an important breakthrough in the research of molecular ferroelectric crystals, di-isopropyl-ammonium halide (DIPAX, X=C (Cl), B (Br), and I) molecular crystals were reported to show ferroelectricity with high curie temperatures, large spontaneous polarizations and low coercive fields. However, their spontaneous polarization is still not sure, as the results reported by different groups are with large deviation [18–23]. Previously, the Curie temperature was elucidated by PCC MD in our group. And the spontaneous polarization was also obtained from both first-principles calculations as 6.8, 6.2, and 5.3 $\mu C/cm^2$ and PCC MD as 5.4±0.3, 5.0±0.4, and 4.0±0.4 $\mu C/cm^2$, respectively [17]. But the ferroelectric hysteresis loops are still unknown. Secondly, salicylideneaniline was recently reported that it has obvious ferroelectricity and photoswitchable performance [24], which opens the gate of photoswitchable ferroelectrics for advanced optoelectronic applications. At last, (-)-camphanic acid was recently prepared as a new organic plastic ferroelectric with a large saturated polarization and high T_C [25]. The mechanisms of ferroelectric switching for all above novel molecular ferroelectrics are still vague and need a systematical study to facilitate their practical applications.

In this work, we use PCC MD to simulate the mechanisms of ferroelectric switching for five characteristic molecular ferroelectrics mentioned above, with their ferroelectric hysteresis loops. Our work can elucidate the ferroelectric switching mechanism for the molecular ferroelectrics, extend the application range of the PCC MD, demonstrate the efficiency and reliability of PCC, and guide the design of novel molecular ferroelectrics, which will promote the application of molecular ferroelectrics in production and life.

II. METHOD

A. Di-isopropyl-ammonium halide molecular crystals

Both the structures and PCC charges of di-isopropyl-ammonium halide molecular crystals (DIPAX) can refer to our previous work [17], and here we just provide a brief summary. We build a 10×10×10 supercell for each system with dimensions of 76.7 Å×79.5 Å×77.7 Å for DIPAC, 78.6 Å×81.0 Å×79.0 Å for DIPAB and 80.1 Å×81.7 Å×80.1 Å for DIPAI respectively. There are 2000 molecules with a total of 48,000 atoms in each supercell, with periodic boundary condition (PBC) imposed on the models. In such systems, for simplicity, we keep the partial charge of halide anions as −1 a.u. (in atomic units), and the whole organic cations with

DOI:10.1063/1674-0068/cjcp2204067

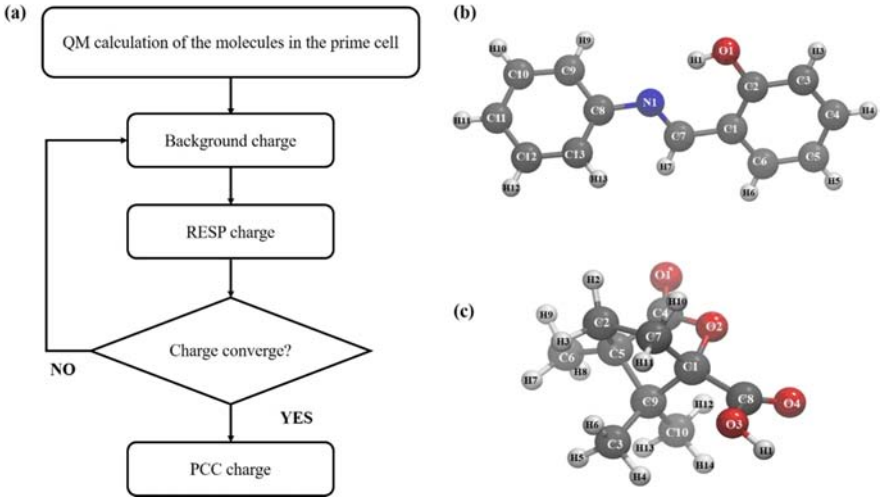

FIG. 1 (a) Flowchart for PPC fitting. (b) The charges of SA calculated by the PCC model and RESCU software. (c) The charges of CA calculated by the PCC model and RESCU software.

charge as +1 a.u.

B. Salicylideneaniline (SA)

The original molecular structure is obtained from the CCDC database [26] with entry ID 2070775. The experimental work reported that SA crystallizes in an orthorhombic polar space group $Fdd2$ [24]. We performed the first-principles calculations to optimize all four kinds of initial structures by the Vienna *Ab initio* Simulation Package (VASP) [27], and then choose the optimized configurations, (shown in FIG. S1 in Supplementary materials, SM) as initial structure for PCC MD simulations. A 5×5×5 super cell with dimensions of 64.8 Å×137.2 Å×29.1 Å for SA is built. There are 1000 molecules with a total of 26,000 atoms in the supercell with PBC.

C. (-)-Camphanic acid (CA)

The original molecular structure is obtained from the experimental work in which CA was reported to crystalize at room temperature in the $P2_1$ space group and 2 (C_2) chiral polar point group [25]. A 7×7×7 supercell with the size of 45.885 Å×77.035 Å×54.733 Å is built, including 686 molecules and 19208 atoms in total with periodic boundary conditions with PBC.

D. Details of MD simulation

The PCC model is incorporated into the force field for the MD simulation, and the other force field parameters are obtained from the generalized AMBER force field (GAFF) [28]. The PCC model takes the molecules other than those in the middle of the supercell as the background, and calculates the charge of the single molecule in the middle of the supercell by the RESP point charge model [29] with the background charges, and then the charge will be updated as a background charge of the system. After several cycles, when the charges converge, the final PCC are obtained. The protocol for fitting PCC is summarized in FIG. 1(a). The PCC charge convergences of SA and CA are shown in FIG. S2 and FIG. S3 in SM, respectively. In addition, we calculate the Mulliken partial charge of the molecule in the large supercell (3×3×3 for SA and 5×5×5 for CA) by first-principles calculations using software named Real space Electronic Structure CalcUlator (RESCU) [30] (PBE with LCAO basis, see SM for details) to have a comparison. We find that the Mulliken charge for the single molecule within supercell is close to the converged PCC one, showing that our method can correctly describe the polarization and screening effect in the crystal. Both of the calculated PCC and Mulliken charges of SA and CA are shown in Tables I and II.

For density functional theory (DFT) calculations of single molecule, we use B3LYP functional [31], with 6-31G(d) basis [32]. All calculations are performed with Gaussian 09 package [33].

The MD simulations are carried out with NAMD package [34]. Each system initially reaches equilibrium in the NPT ensemble where the temperature is 418 K (DIPAX, X=C (Cl), B (Br), and I) or 300 K (SA and

DOI:10.1063/1674-0068/cjcp2204067

TABLE I The charges of SA calculated by the PCC model and RESCUE software.

Atom	PCC	RESCU	Atom	PCC	RESCU
O1	−0.4815	−0.9394	C13	−0.1700	−0.1417
C1	−0.0294	0.0128	H1	0.3228	0.7500
C2	0.2727	0.1645	H3	0.1861	0.2145
C3	−0.2277	−0.1674	H4	0.1548	0.0505
C4	−0.1045	−0.1125	H5	0.1349	0.1344
C5	−0.2002	−0.1268	H6	0.1754	0.1154
C6	−0.1897	−0.1304	H7	0.0577	0.2108
C7	0.0930	−0.1719	H9	0.1349	0.1766
C8	0.1609	0.0386	H10	0.1413	0.1397
C9	−0.1700	−0.1398	H11	0.1654	0.1002
C10	−0.1278	−0.1282	H12	0.1413	0.1339
C11	−0.1707	−0.1185	H13	0.1278	0.1275
C12	−0.1278	−0.1264	N1	−0.3510	−0.0663

TABLE II The charges of CA calculated by the PCC model and RESCUE software.

Atom	PCC	RESCU	Atom	PCC	RESCU
O1	−0.6012	−0.6393	H1	0.5065	0.9337
O2	−0.5134	−0.2807	H2	0.0859	0.0984
O3	−0.6237	−0.7628	H3	0.0859	0.1605
O4	−0.5197	−0.6844	H4	0.1347	0.1055
C1	0.3891	0.1455	H5	0.1347	0.1247
C2	−0.1176	−0.1791	H6	0.1347	0.1197
C3	−0.5180	−0.2755	H7	0.1262	0.1162
C4	0.6875	0.4618	H8	0.1262	0.1043
C5	0.0669	0.0080	H9	0.1262	0.1079
C6	−0.4269	−0.2761	H10	0.0994	0.1495
C7	−0.2221	−0.1969	H11	0.0994	0.1829
C8	0.5687	0.3884	H12	0.1347	0.1102
C9	0.2842	0.0349	H13	0.1347	0.1000
C10	−0.5180	−0.2734	H14	0.1347	0.1161

CA), and the pressure is 1 atm. To keep the temperature and the pressure constant, we use Langevin dynamics thermostat [35] and Nose-Hoover piston barostat [36, 37]. In particular, in the simulation of CA, the SHAKE algorithm [38] is used for all covalence bonds involving hydrogen atoms. When applying an external electric field to the system in the NVT ensemble, we run several independent trajectories to study the process of polarization switching more clearly, where the system polarization values are collected every 2 ps. Long-range electrostatic interactions are treated with the particle mesh Ewald method [39] where the grid size is 1 Å, and the cutoff of van der Waals interaction [40] is 12 Å. During the simulation processes, the time step of CA is set to 2 fs, and the time step of other systems is all set to 1 fs. The Visual Molecular Dynamics (VMD) [41] package is used for data analysis.

III. RESULTS AND DISCUSSION

A. DIPAX molecular crystals

The primitive cells of the crystal structures of DIPAC, DIPAB and DIPAI are shown in FIG. 2(a−c). Structures and PCC charge parameters refer to our previous work [17].

To understand the ferroelectric switching mechanism of DIPAX, we examine the response of the crystal structure and polarization under the external electric field E at 418 K as experimentally used [18, 19]. During the MD simulation, the direction of E is all set along the y-axis, and its magnitudes of DIPAC and DIPAI increase from 0 to 6 kV/cm, then decrease to −6 kV/cm inversely, and then return to 0 kV/cm. The E of DIPAB increases from 0 to 4 kV/cm, then decreases to −4 kV/cm inversely, and then finally returns to zero.

The results of electric hysteresis loops of DIPAC, DIPAB, and DIPAI are shown in FIG. 2(d−f). As shown in the figure, when $|E|$ increases to 6 kV/cm (DIPAC and DIPAI) or 4 kV/cm (DIPAB), the saturated spontaneous polarization (P_s) values of DIPAC, DIPAB and DIPAI are 6.1±0.2 μC/cm^2, 6.3±0.1 μC/cm^2, and 5.0±0.1 μC/cm^2, respectively. To the best of our knowledge, different groups reported different P_s, for which the value of DIPAC ranges from 5.4 μC/cm^2 to 10.5 μC/cm^2, the value of DIPAB ranges from 3.5 μC/cm^2 to 20.5 μC/cm^2 and the value of DIPAI ranges from 5.2 μC/cm^2 to 33.0 μC/cm^2 [18−23]. Our results in this work are highly compatible with our first-principles results as 6.8, 6.2, and 5.3 μC/cm^2, respectively [17]. The reason of large deviation among different results is still in puzzle. The relative deviations between our PCC MD results and first-principles results are about 10%, 2% and 6%. From the simulated ferroelectric hysteresis loops, the E_c values of DIPAC and DIPAI are 2.1 kV/cm and 2.9 kV/cm, and to our surprise, the E_c value of DIPAB is only 0.3 kV/cm. They are all smaller than the values obtained in experimental work, for which the value of DIPAC ranges from 5 kV/cm to 10 kV/cm, the value of DIPAB ranges from 5 kV/cm to 12 kV/cm and the value of DIPAC is 12 kV/cm [18−23]. Considering PCC can give highly

DOI:10.1063/1674-0068/cjcp2204067

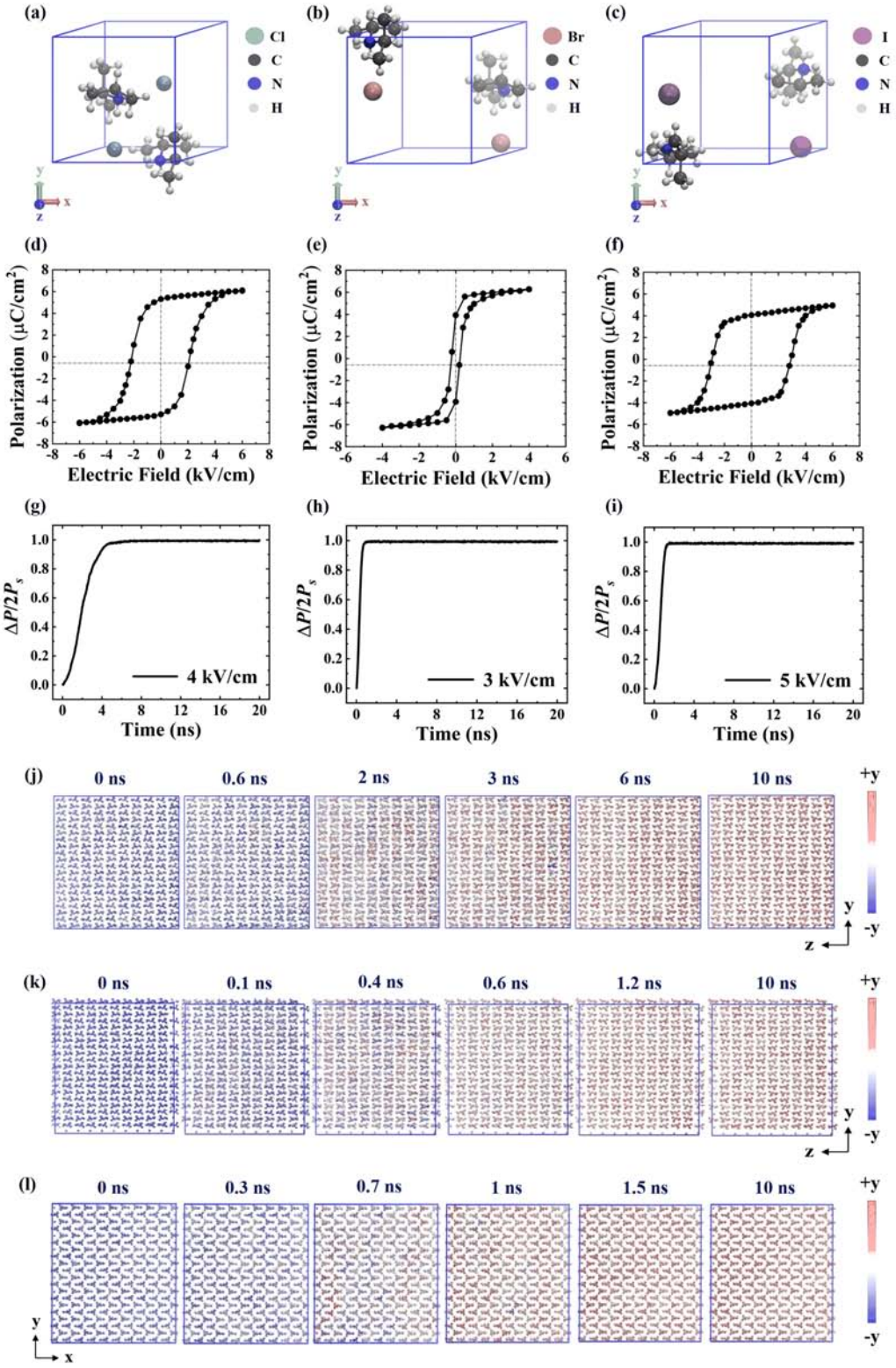

FIG. 2 Prime cell of (a) DIPAC, (b) DIPAB and (c) DIPAI. Ferroelectric hysteresis loop of (d) DIPAC, (e) DIPAB, and (f) DIPAI from PCC MD simulation at 418 K. Time-dependent evolution of the growing domain during the switching process of (g) DIPAC in an external electric field of 4 kV/cm, (h) DIPAB in an external electric field of 3 kV/cm, and (i) DIPAI in an external electric field of 5 kV/cm. Process of polarization switching of (j) DIPAC in an external electric field of 4 kV/cm, (k) DIPAB in an external electric field of 3 kV/cm, and (l) DIPAI in an external electric field of 5 kV/cm. The red and blue regions represent different directions of polarization, corresponding to domains with $+y$ and $-y$ directions of their molecular dipoles.

DOI:10.1063/1674-0068/cjcp2204067

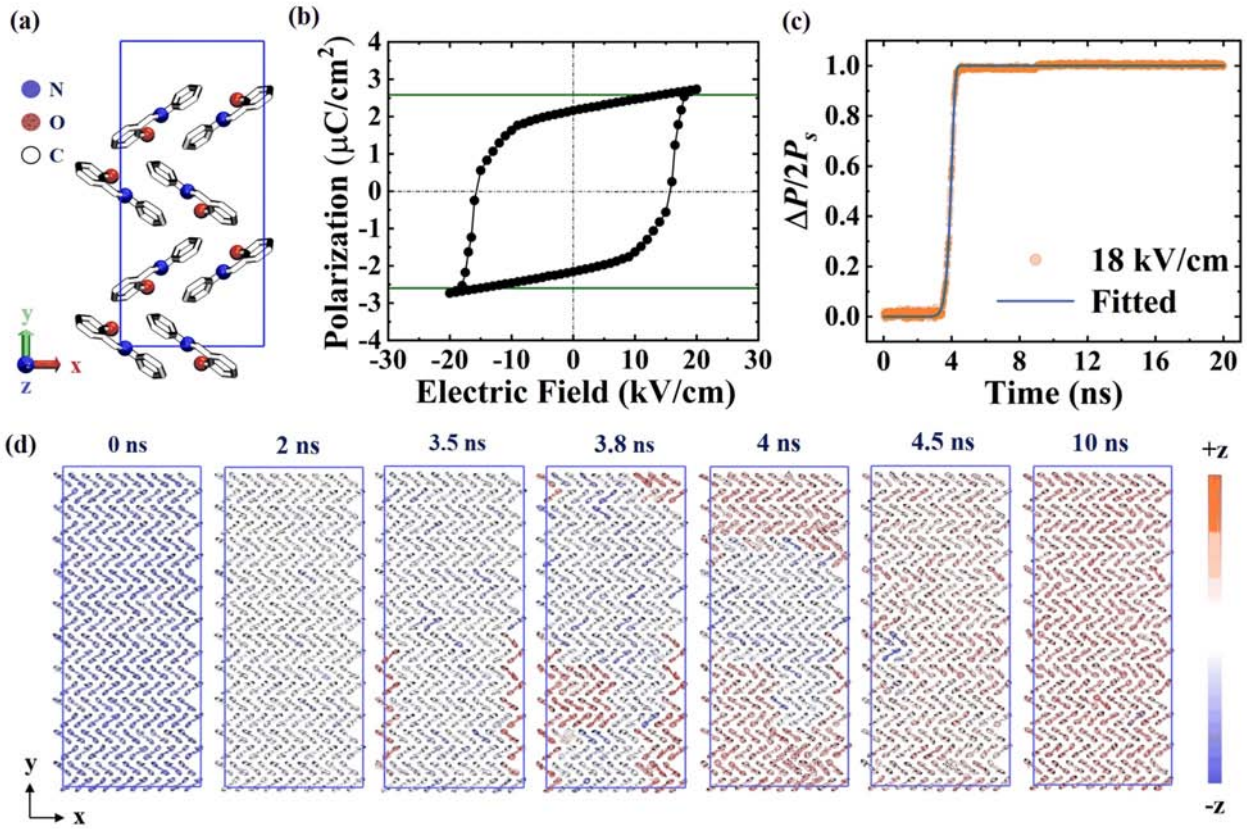

FIG. 3 (a) Prime cell of SA, H atoms are omitted for clarity. (b) Ferroelectric hysteresis loop by PCC MD simulation at 300 K. The horizontal green line marks the sum of dipoles from isolated molecules. (c) Time-dependent evolution of the growing domain during the switching process under the external electric field of 18 kV/cm, shown as orange dots, with the solid lines corresponding to results fitted by KAI model. (d) Process of polarization switching of SA crystal in an external electric field of 18 kV/cm. The red and blue regions represent different directions of polarization, corresponding to domains with $+z$ and $-z$ directions of their molecular dipoles.

compatible E_c in our previous findings [15, 16], we hope further experiments can settle down the mismatch of E_c.

The P_s evolving with time is plotted in FIG. 2(g−i) to depict details of the polarization switching of DIPAC, DIPAB and DIPAI crystal, and the simulation is under the external electric field of 4 kV/cm, 3 kV/cm, and 5 kV/cm, respectively. From the plots, polarizations of DIPAC, DIPAB,and DIPAI crystal start to change nearly immediately after applying the external electric field, and reach their saturation polarization values after 6 ns, 1.2 ns, and 1.5 ns, respectively. These process can also be visualized at the molecular level by FIG. 2(j−l). During the simulation, multiple domains randomly emerge, grow to fill the super cell, and at last reach saturation. The total process occurs homogeneously in space. For the microscopic mechanism of the polarization switching, when a sufficiently large external electric field is applied, the orientation of the -NH_2 group of the DIPAX molecules flips along the y-axis, leading to the spontaneous polarization changes accordingly.

B. Salicylideneaniline

The prime cell of crystal structures of SA contains eight molecules, as shown in FIG. 3(a). As in the work of croconic acid [42], we have calculated the dipole moment of isolated SA molecule using DFT. The calculated value was 2.264 Debye, similar to the previously reported result [24].

To understand the origin of ferroelectricity of SA, we examine the response of the crystal structure and polarization under external electric field E at 300 K as experimentally used [24]. During the MD simulation, the direction of E is set along the z-axis, and its magnitude varies from 0 to 20 kV/cm, then decreases to −20 kV/cm inversely, then finally returns to 0 kV/cm.

DOI:10.1063/1674-0068/cjcp2204067

The result of electric hysteresis loop of SA is shown in FIG. 3(b). As shown in the figure, the $|P_s|$ value of 2.74±0.1 μC/cm^2 can be obtained after applying the external electric field E of 20 kV/cm. When the E reverses, the polarization switches accordingly to −15.5 kV/cm and then reaches its reversed saturate value at −20 kV/cm. Such results are highly compatible with the polarization value estimated by first-principles calculations, which was 2.71 μC/cm^2, and slightly higher than experimental results, P_s=1.95 μC/cm^2 at room temperature [24], and the relative deviation is about 1% and 41% respectively. Here the sum of dipoles from single molecules within a single cell is also obtained as 2.58 μC/cm^2, shown as horizontal green lines in the FIG. 3(b). The single molecular dipole moment is lower than the crystalline polarization, suggesting that intermolecular polarization effect is relevant. From the simulated ferroelectric hysteresis loop, the E_c is 15.5 kV/cm. Here one should notice that both the first-principles calculations and our PCC MD simulations are for bulk system, while in the experiments the thin films are under measurements, and such difference would contribute deviation between results from calculations and experiments.

The P_s evolving with time is plotted in FIG. 3 (c) and (d) to depict details of the polarization switching of a 5×5×5 supercell of the SA crystal. The result is obtained from PCC MD under the external electric field of 18 kV/cm along the z-axis at 300 K with constant volume. There are two stages in the process of SA polarization switching. After applying the external electric field, the polarization value of SA first equilibrates for a period of 3.5 ns, and then the polarization starts to increase and reaches the saturation value within 1 ns. At molecular level, this process can be recognized in FIG. 3(d). One can observe that SA molecules first equilibrates for a period of time till 3.5 ns, and then a single domain randomly emerges. Such domain grows to fill the super cell after 4.5 ns, and at last reaches saturation till 10 ns. Since this process satisfies a fundamental assumption of the Kolmogorov-Avrami-Ishibashi (KAI) model [43] that only one domain exists throughout the switching process, we try to fit the evolution of spontaneous polarization with time to the KAI model in FIG. 3(c).

The KAI model is with the functional form:

$$\Delta P(t) = P(t) - P(0) = 2P_s[1 - e^{-(t/t_0)^n}] \quad (1)$$

It contains three fitted parameters, P_s corresponds to the saturated spontaneous polarization, t_0 is characteristic time, and n is related to the dimensionality, ranging from 1 to 4.

The fitted values are P_s=1.362, t_0=4.026 and n=19.92 respectively. Here we can see although our simulated data fits the fitted functional form at first glance, the fitted parameter n exceeds the predicted range, which may be caused by inhomogeneity, so the polarization switching process of SA cannot be explained by KAI model. This phenomenon is similar to our previous work [16], reflecting again the polarization switching process of molecular crystals is inherently complex, and a new model for describing such kind of process is needed. For the microscopic mechanism of the polarization switching, both C−O and C−N bonds in each molecule within the supercell to the same side generate spontaneous polarization along the z-axis. When a sufficiently large external electric field is applied, the body of SA molecules will rotate along C1−C8 axis by about 180°, so the polarization direction will also be flipped (atoms are labelled in FIG. 1(b)).

C. (-)-Camphanic acid

The prime cell of crystal structures of CA is shown in FIG. 4(a). It contains two molecules, and the dipole moment of the single CA molecule is 6.165 Debye.

To understand the ferroelectric switching mechanism of CA, we examine the response of the crystal structure and polarization under external electric field E at 300 K as experimentally used [25]. During the MD simulation, the direction of E is set along the y-axis, and the magnitude varies from 0 to 10 kV/cm, then decreases to −10 kV/cm inversely, then finally back to 0 kV/cm.

The result of electric hysteresis loop is shown in FIG. 4(b). The $|P_s|$ value of 6.8±0.4 μC/cm^2 can be obtained after applying an electric field of 10 kV/cm. When the E reversed, the polarization switches accordingly to −7 kV/cm and then reaches a reversed saturate value after $|E|$ increases to 10 kV/cm. Such results are slightly higher than experimental results, P_s=5.2 μC/cm^2 at room temperature [25], and the relative error is about 31%. Here the sum of dipoles from single molecules within a single cell is also obtained as about 4.91 μC/cm^2, as shown as horizontal green lines in the FIG. 4(b). The single molecular dipole moment is lower than the crystalline polarization, suggesting that intermolecular polarization effect is relevant.

DOI:10.1063/1674-0068/cjcp2204067

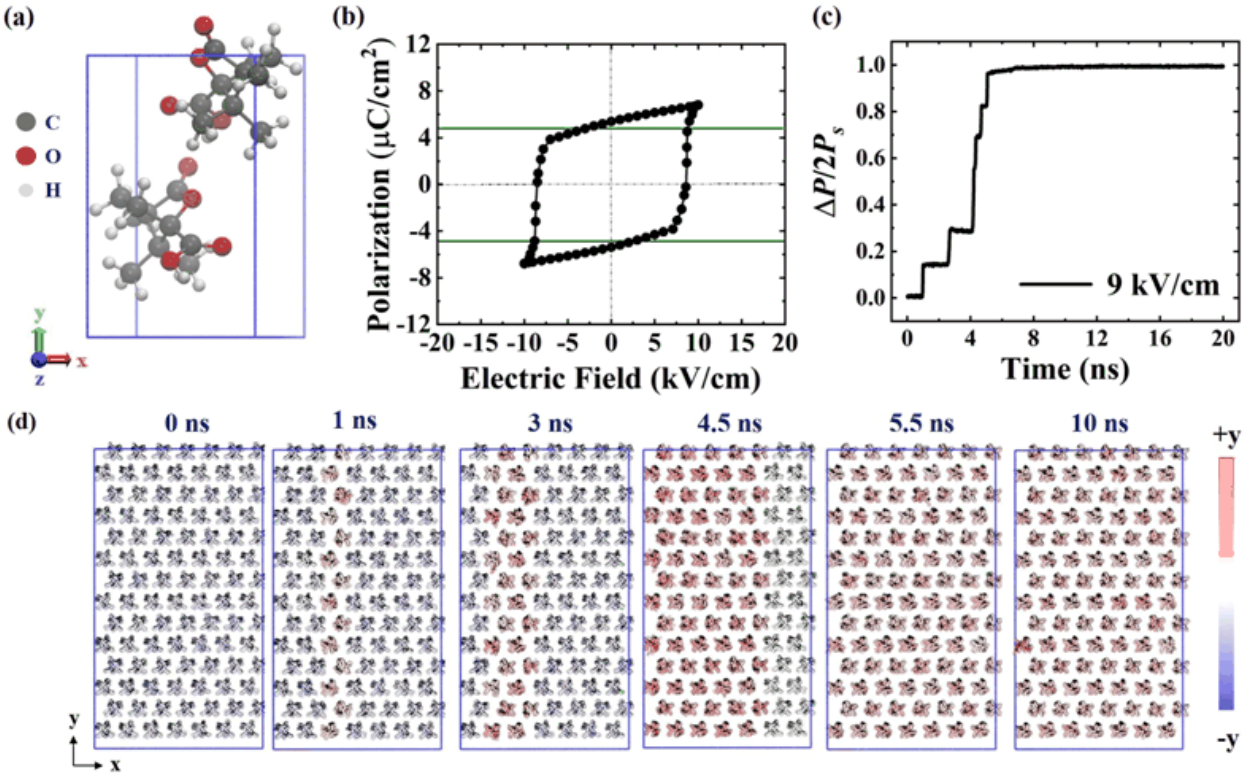

FIG. 4 (a) Prime cell of CA. (b) Ferroelectric hysteresis loop from MD simulation using PCC at 300 K. The horizontal green line marks the sum of dipoles from isolated molecules. (c) Time-dependent evolution of the growing domain during the switching process under the external electric field of 9 kV/cm. (d) Process of polarization switching of CA in an external electric field of 9 kV/cm. The red and blue regions represent different directions of polarization, corresponding to domains with $+y$ and $-y$ directions of their molecular dipoles.

From the simulated ferroelectric hysteresis loop, the E_c is 8.5 kV/cm, which is much smaller than the experimentally obtained E_c of 50 kV/cm. As discussed in the above, the simulated system is bulk crystal, while in experiments thin films are used. Such difference would contribute the deviation between simulated results and experimental ones.

The P_s evolving with time is plotted to depict details of the polarization switching of a 7×7×7 supercell of the CA crystal in FIG. 4 (c) and (d). The simulation is under the external electric field of 9 kV/cm along the y-axis at 300 K with constant volume. Interestingly, the polarization switching occurs spontaneously from one strip-shaped domain to the neighboring domain one-by-one, until fully saturated at last. Such process is depicted by the steps in the P_s-time plot FIG. 4(c), and can also be visualized at the molecular level by FIG. 4(d). A strip-shaped domain randomly emerges at about 1.0 ns, grows to fill the super cell until 6 ns, and at last reaches saturation till 10 ns. For the microscopic mechanism of the polarization switching, when a sufficiently large external electric field is applied, the body of the CA molecule will rotate along C6−C8 axis about 60°, and the carboxyl group (-COOH) will rotate separately 180° along the same axis, thus the polarization direction will also be flipped (atoms are labelled in the FIG. 1(c)).

IV. CONCLUSION

In summary, we use PCC MD method to simulate the mechanism of ferroelectric switching of (DIPAX, X=C (Cl), B (Br), and I), SA, and CA under applied external electric fields. From our results, the spontaneous polarizations, coercive fields, ferroelectric hysteresis loops, and corresponding switching mechanisms are obtained. We find that the spontaneous polarizations of DIPAC, DIPAB and DIPAI are 6.1, 6.3, and 5.0 μC/cm^2 respectively, and the corresponding E_c values of DIPAC, DIPAB, and DIPAI are 2.1, 0.3, and 2.9 kV/cm. We also find that SA crystals have a spontaneous polarization of 2.7 μC/cm^2, and its E_c is 15.5 kV/cm. The P_s of CA is 6.8 μC/cm^2 and the E_c is 8.5 kV/cm. Results

DOI:10.1063/1674-0068/cjcp2204067

show that, PCC MD method can efficiently simulate the ferroelectric switching process of molecular ferroelectrics and give moderate accuracy results [44], which will help to better elucidate its mechanism and further promote the practical application of molecular ferroelectricity. The deviation between our results and the experimental results may be from the following reasons: the experimental and simulated conditions are not exactly the same, the experiment errors, and the force field errors. Firstly the fixed partial charges during dynamic simulations would bring considerable error, a polarizable force field, such as AMOEBA [45, 46], would alleviate such kind of deficiency. Secondly, although we consider electrostatic polarization by the PCC model, other force field parameters are obtained from the generalized AMBER force field (GAFF) [28], which are established based on the behavior of molecules in aqueous solutions and may not be suitable for simulations in crystals. Among them, the van der Waals interaction parameters in particular may require to be further revised, which will be the goal of our future method improvement. After all, this work expands the application range of PCC MD and demonstrates the efficiency and reliability of the method, hoping that our method can serve as an effective tool for the study of molecular ferroelectrics and promote the continuous development of molecular ferroelectrics.

Supplementary materials: Energy comparison of the four initial structures of SA is shown. The PCC charge convergence of SA and CA, and the calculation details of the Mulliken partial charge calculated by RESCU are available.

V. ACKNOWLEDGMENTS

This work is funded by the National Natural Science Foundation of China (No.22173057) and the research grant (No.21JC1402700) from Science and Technology Commission of Shanghai Municipality. This work is also supported by the Key Research Project of Zhejiang Laboratory (No.2021PE0AC02). We appreciate the Ziqiang 4000 of Shanghai University for high-performance computing services, and we gratefully acknowledge HZWTECH for providing computation facilities.

[1] H. Lu, C. W. Bark, D. Esque de los Ojos, J. Alcala, C. B. Eom, G. Catalan, and A. Gruverman, Science **336**, 59 (2012).

[2] P. Maksymovych, S. Jesse, P. Yu, R. Ramesh, P. Baddorf Arthur, and V. Kalinin Sergei, Science **324**, 1421 (2009).

[3] B. Neese, B. Chu, S. G. Lu, Y. Wang, E. Furman, and Q. M. Zhang, Science **321**, 821 (2008).

[4] J. F. Scott, Science **315**, 954 (2007).

[5] S. Zhang and F. Yu, J. Am. Ceram. Soc. **94**, 3153 (2011).

[6] S. H. Baek, J. Park, D. M. Kim, V. A. Aksyuk, R. R. Das, S. D. Bu, D. A. Felker, J. Lettieri, V. Vaithyanathan, S. S. N. Bharadwaja, N. Bassiri-Gharb, Y. B. Chen, H. P. Sun, C. M. Folkman, H. W. Jang, D. J. Kreft, S. K. Streiffer, R. Ramesh, X. Q. Pan, S. Trolier-McKinstry, D. G. Schlom, M. S. Rzchowski, R. H. Blick, and C. B. Eom, Science **334**, 958 (2011).

[7] H. Y. Ye, Y. Y. Tang, P. F. Li, W. Q. Liao, J. X. Gao, X. N. Hua, H. Cai, P. P. Shi, Y. M. You, and R. G. Xiong, Science **361**, 151 (2018).

[8] A. Stroppa, P. Jain, P. Barone, M. Marsman, J. M. Perez-Mato, A. K. Cheetham, H. W. Kroto, and S. Picozzi, Angew. Chem. Int. Ed. **50**, 5847 (2011).

[9] J. Li, Y. Liu, Y. Zhang, H. L. Cai, and R. G. Xiong, Phys. Chem. Chem. Phys. **15**, 20786 (2013).

[10] Y. Li, W. Fan, X. Li, W. Ren, and Y. Li, Chin. J. Chem. Phys. **34**, 843 (2021).

[11] D. A. Case, T. E. Cheatham Iii, T. Darden, H. Gohlke, R. Luo, K. M. Merz Jr., A. Onufriev, C. Simmerling, B. Wang, and R. J. Woods, J. Comput. Chem. **26**, 1668 (2005).

[12] J. B. Klauda, R. M. Venable, J. A. Freites, J. W. O'Connor, D. J. Tobias, C. Mondragon-Ramirez, I. Vorobyov, A. D. MacKerell, and R. W. Pastor, J. Phys. Chem. B **114**, 7830 (2010).

[13] T. Zhu, C. Wu, J. Song, J. R. Reimers, and Y. Li, Chem. Phys. Lett **706**, 303 (2018).

[14] Y. Li, J. Z. H. Zhang, and Y. Mei, J. Phys. Chem. B **118**, 12326 (2014).

[15] P. Hu, S. Hu, Y. Huang, J. R. Reimers, A. M. Rappe, Y. Li, A. Stroppa, and W. Ren, J. Phys. Chem. Lett. **10**, 1319 (2019).

[16] X. Zhu, W. Fan, W. Ren, and Y. Li, J. Phys. Chem. C **125**, 12461 (2021).

[17] Y. Huang, P. Hu, J. Song, Y. Li, and A. Stroppa, Chem. Phys. Lett. **730**, 367 (2019).

[18] D. W. Fu, W. Zhang, H. L. Cai, J. Z. Ge, Y. Zhang, and R. G. Xiong, Adv. Mater. **23**, 5658 (2011).

[19] D. W. Fu, H. L. Cai, Y. Liu, Q. Ye, W. Zhang, Y. Zhang, X. Y. Chen, G. Giovannetti, M. Capone, J. Li, and R. G. Xiong, Science **339**, 425 (2013).

[20] R. K. Saripalli, D. Swain, S. Prasad, H. Nhalil, H. L. Bhat, T. N. G. Row, and S. Elizabeth, J. Appl. Phys. **121**, 114101 (2017).

[21] C. Thirmal, P. P. Biswas, Y. J. Shin, T. W. Noh, N. V. Giridharan, A. Venimadhav, and P. Murugavel, J. Appl. Phys. **120**, 124107 (2016).
[22] A. Piecha, A. Gągor, R. Jakubas, and P. Szklarz, CrystEngComm **15**, 940 (2013).
[23] L. Louis, K. C. Pitike, A. Ghosh, S. Poddar, S. Ducharme, and S. M. Nakhmanson, J. Mater. Chem. C **6**, 1143 (2018).
[24] Z. X. Wang, C. R. Huang, J. C. Liu, Y. L. Zeng, and R. G. Xiong, Chem. Eur. J. **27**, 14831 (2021).
[25] Y. Ai, P. F. Li, M. J. Yang, Y. Q. Xu, M. Z. Li, and R. G. Xiong, Chem. Sci. **13**, 748 (2022).
[26] F. H. Allen, S. Bellard, M. D. Brice, B. A. Cartwright, A. Doubleday, H. Higgs, T. Hummelink, B. G. Hummelink-Peters, O. Kennard, W. D. S. Motherwell, J. R. Rodgers, and D. G. Watson, Acta Cryst. B **35**, 2331 (1979).
[27] J. Hafner, J. Comput. Chem. **29**, 2044 (2008).
[28] J. Wang, R. M. Wolf, J. W. Caldwell, P. A. Kollman, and D. A. Case, J. Comput. Chem. **25**, 1157 (2004).
[29] C. I. Bayly, P. Cieplak, W. Cornell, and P. A. Kollman, J. Phys. Chem. **97**, 10269 (1993).
[30] V. MichaudRioux, L. Zhang, and H. Guo, J. Comput. Phys. **307**, 593 (2016).
[31] A. D. Becke, J. Chem. Phys. **98**, 5648 (1993).
[32] A. D. McLean and G. S. Chandler, J. Chem. Phys. **72**, 5639 (1980).
[33] M. J. Frisch, G. W. Trucks, H. B. Schlegel, G. E. Scuseria, M. A. Robb, J. R. Cheeseman, G. Scalmani, V. Barone, B. Mennucci, G. A. Petersson, H. Nakatsuji, M. Caricato, X. Li, H. P. Hratchian, A. F. Izmaylov, J. Bloino, G. Zheng, J. L. Sonnenberg, M. Hada, M. Ehara, K. Toyota, R. Fukuda, J. Hasegawa, M. Ishida, T. Nakajima, Y. Honda, O. Kitao, H. Nakai, T. Vreven, J. A. Jr. Montgomery, J. E. Peralta, F. Ogliaro, M. Bearpark, J. J. Heyd, E. Brothers, K. N. Kudin, V. N. Staroverov, R. Kobayashi, J. Normand, K. Raghavachari, A. Rendell, J. C. Burant, S. S. Iyengar, J. Tomasi, M. Cossi, N. Rega, N. J. Millam, M. Klene, J. E. Knox, J. B. Cross, V. Bakken, C. Adamo, J. Jaramillo, R. Gomperts, R. E. Stratmann, O. Yazyev, A. J. Austin, R. Cammi, C. Pomelli, J. W. Ochter-ski, R. L. Martin, K. Morokuma, V. G. Zakrzewski, G. A. Voth, P. Salvador, J. J. Dannenberg, S. Dapprich, A. D. Daniels, Ö. Farkas, J. B. Foresman, J. V. Ortiz, J. Cioslowski, and D. J. Fox, *Gaussian 09, Revision A02*, Wallingford, CT: Gaussian Inc., (2009).
[34] M. T. Nelson, W. Humphrey, A. Gursoy, A. Dalke, L. V. Kalé, R. D. Skeel, and K. Schulten, Int. J. Supercomput. Appl. High Perform. Comput. **10**, 251 (1996).
[35] R. W. Pastor, B. R. Brooks, and A. Szabo, Mol. Phys. **65**, 1409 (1988).
[36] S. Nosé and M. L. Klein, Mol. Phys. **50**, 1055 (1983).
[37] M. Bernasconi, G. L. Chiarotti, P. Focher, S. Scandolo, E. Tosatti, and M. Parrinello, J. Phys. Chem. Solids **56**, 501 (1995).
[38] J. P. Ryckaert, G. Ciccotti, and H. J. C. Berendsen, J. Comput. Phys. **23**, 327 (1977).
[39] K. Nam, J. Gao, and D. M. York, J. Chem. Theory Comput. **1**, 2 (2005).
[40] J. P. Hansen and L. Verlet, Phys. Rev. **184**, 151 (1969).
[41] W. Humphrey, A. Dalke, and K. Schulten, J. Mol. Graphics **14**, 33 (1996).
[42] S. Horiuchi, Y. Tokunaga, G. Giovannetti, S. Picozzi, H. Itoh, R. Shimano, R. Kumai, and Y. Tokura, Nature **463**, 789 (2010).
[43] A. K. Tagantsev, I. Stolichnov, N. Setter, J. S. Cross, and M. Tsukada, Phys. Rev. B **66**, 214109 (2002).
[44] T. E. Smidt, S. A. Mack, S. E. Reyes-Lillo, A. Jain, and J. B. Neaton, Sci. Data **7**, 72 (2020).
[45] P. Ren and J. W. Ponder, J. Comput. Chem. **23**, 1497 (2002).
[46] P. Ren and J. W. Ponder, J. Phys. Chem. B **107**, 5933 (2003).

DOI:10.1063/1674-0068/cjcp2204067